AN INVESTIGATION OF THE MAXIMUM TARGET MATERIAL SPRAY VELOCITY PRODUCED IN THE PENETRATION OF THIN PLATES BY HIGH VELOCITY DISKS

By

John D. Di Battista

Thesis submitted to the Graduate Faculty of the

Virginia Polytechnic Institute

in candidacy for the degree of

MASTER OF SCIENCE

in

ENGINEERING MECHANICS

June 1966

AN INVESTIGATION OF THE MAXIMUM TARGET MATERIAL SPRAY VELOCITY PRODUCED IN THE PENETRATION OF THIN PLATES BY HIGH VELOCITY DISKS

by

John D. Di Battista

Thesis submitted to the Graduate Faculty of the

Virginia Polytechnic Institute

in candidacy for the degree of

MASTER OF SCIENCE

in

ENGINEERING MECHANICS

APPROVED:

Chairman, R. Thomas Davis

H. F. Brinson

R. P. McNitt

June 1966

Blacksburg, Virginia

II. TABLE OF CONTENTS

III. LIST OF FIGURES AND TABLE

FIGURE PAGE

TABLE

IV. INTRODUCTION

The meteoroid bumper is a thin sheet of material placed at some distance in front of a spacecraft's main wall and is used to protect the spacecraft from high velocity meteoroids. Its function is to break up an impacting meteoroid and produce a diverging spray of small meteoroid and meteoroid bumper particles. The diverging spray of smaller particles is less damaging to the main wall of the spacecraft than is the original meteoroid.

The analysis of the impact penetration of a spacecraft's main wall when protected by a bumper is an extremely difficult problem. The problem can best be approached in two phases. The first phase of the analysis deals with the penetration of the bumper to establish the particle sizes and velocities of the spray exiting from the rear of the bumper. The second phase of the analysis deals with the damage to be inflicted on the main wall by the impact of this debris. The analytical and experimental data reported herein involve only the penetration of the bumper and, in particular, determine the maximum velocity of the meteoroid bumper spray particles which strike the main wall.

An experimental technique is employed to produce a one-dimensional interaction between a thin target and an impacting projectile so that an analysis of the maximum meteoroid bumper material spray velocity can be carried out. To this end the projectile used is disk shaped and is allowed to impact only on its face with thin targets. The projectile target material combination chosen is tungsten for the projectiles and aluminum for the targets. By using a projectile material much denser

than the target material, the projectile and the leading target material spray positions are clearly discernible after impact in the photographic data. The reason for this clarity of positions is that the leading target material spray velocity is well in excess of the projectile impact velocity. The experimentally determined ratio of the maximum target material spray velocity and projectile impact velocity is compared to the analytically predicted ratio over the impact velocity range tested.

V. SYMBOLS

C'	empirical constant, cm/μsec
C''	empirical constant, dimensionless
P	pressure
U	velocity
ρ	density

Subscripts:

c	compressed material after shock-wave passage
e	rarefaction wave
f	target rear surface
o	uncompressed material before shock-wave passage
p	projectile
r	expanded material after rarefaction passage
s	shock wave
t	target

VI. REVIEW OF LITERATURE

Davidson and Sandoff (ref. 3) have made a study of the meteoroid environment (i.e., velocity, mass, and size distribution) and its danger to spacecraft. Their work shows that to have successful space flights a method of meteoroid protection must be found for spacecraft. Such a method, the meteoroid bumper, was first proposed by Frederick L. Whipple (ref. 10) and was verified by Donald H. Humes (ref. 6) to protect spacecraft against penetration by hypervelocity meteoroids. The bumper uses the energy of the impacting meteoroid to fragment or vaporize the meteoroid and produces a diverging spray of meteoroid and bumper material particles which is less damaging to the spacecraft's main wall than is the original meteoroid. For the concept of the meteoroid bumper to be of value, the total weight per unit area of penetrated material for the meteoroid bumper and main wall configuration has to be less than the weight per unit area of penetrated material for a single walled structure when the meteoroid impact conditions are the same. As impact velocity is increased to 1 cm/μsec, the limit of our projection devices, the meteoroid bumper and main wall become increasingly superior to the single walled structure.

For the general case of high velocity impact between projectile and thin target it is, at present, impossible to analytically predict what damage the fragments produced will do to the main wall. The reason lies in the fact that neither the velocity nor particle size of projectile and bumper material spray produced from the impact may be analytically determined. The analytical and experimental work done in

this thesis is concerned with the interaction of a projectile and thin plate during collision to determine the maximum spray velocity of the bumper material. The thesis also includes photographs showing the shattered bumper material on the leading edge of the spray cloud.

VII. APPARATUS AND TEST TECHNIQUE

Projectiles and Targets

The projectiles are disks 0.56 cm in diameter and are either 0.076- or 0.038-cm-thick. They are cut using an electrical discharge machining process from 0.076- and 0.038-cm-thick tungsten plate. The tungsten plate is produced by rolling operations on a tungsten ingot which is produced with powdered metallurgy techniques from pure metal powder with a minimum tungsten content of 99.95 percent. The density of the tungsten is 19.26 gm/cm^3.

The tungsten disk projectiles are loaded into the accelerator after mounting on nylon sabots of length-to-diameter ratios of either 1 or 1/2. These sabots are sufficient to prevent shattering of the projectile during launch. Figure 1 shows the mounting of the 0.076-cm-thick tungsten disk on a sabot of length-to-diameter ratio 1 and the 0.038-cm-thick tungsten disk on a sabot of length-to-diameter ratio 1/2.

The targets are made of 1100 aluminum foil which is 0.0025-cm-thick and 1100 H14 aluminum plate which is 0.041-cm-thick.

Accelerators

Two projectile accelerators are used in the experimental investigation. A conventional 22-caliber Swift rifle is used to accelerate projectiles in the velocity range of 0.089 to 0.219 cm/μsec. A shock compressed helium gas gun is used to accelerate projectiles in the range of 0.219 to 0.295 cm/μsec. A description and photograph of each of these accelerators is presented in reference 2.

Methods of Measuring Velocity of Projectile and Spray

Two methods are used to determine the projectile velocity. The first method uses two projectile detection stations 60.9 cm apart. When the projectile appears at the first station, it passes through a light beam and reflects some of the light into a receiving photomultiplier which then sends a signal to an electronic time interval meter to begin counting. The same photomultiplier also sends a signal to an image converter photographing system to take a picture of the projectile. At the second station the same procedure is repeated with the time interval meter being stopped. This system gives all the information necessary to determine the projectile velocity. The accuracy of this system is estimated to be better than ±3 percent. Figure 2 shows two photographs of the tungsten disk taken at the start and stop stations of the system.

The second method of determining the projectile velocity uses a high-speed framing camera. The velocity of the target material spray is also determined with this camera. The time between frames on the film record is computed from the recorded period of rotation of the spinning inner mirror of the camera at the time of projectile impact. A film reader is then used to make measurements of the projectile positions and target spray positions on the 35-mm film. The film reader magnifies the film record four times its image size and projects it on a screen with a horizontal and vertical grid. The film is then alined horizontally and vertically on the screen with a 1.27-cm-diameter machined cylinder placed in the high-speed framing camera's field of

view. The cylinder is used as a reference point from which measurements are made to either the projectile or spray front on successive frames. On making measurements of the diameter of the machined cylinder, the repeatability of measurements is within 2.50 percent. The velocity of the projectile and spray front is then calculated from the known time between frames and the measured distance traveled between frames. The average percent difference between the two methods of measuring the projectile velocity is 3.18 percent for all shots based on the detection system velocity.

Test Setup and Operation

Figure 3 is a schematic drawing of the complete test setup and includes one of the previously mentioned projectile accelerators. Downstream from the accelerator are located two large blast chambers with a baffle plate between them to eliminate extraneous gun debris from interfering with the experiment. The two detection stations, used to determine the projectile velocity, are located beyond these two blast chambers. The image converter photographing system at each station is placed so as to obtain a top view of the projectile and to be perpendicular to the projectile line of flight. From the data taken at the two detection stations it is verified that the projectile started and stopped the time interval meter. Also, the projectile velocity and the projectile integrity are determined. A time delay computer then uses the time recorded by the detection system to synchronize the 60 μsec duration xenon flash tube with the arrival of the projectile at the target position. The thin target is placed with its flat surface

perpendicular to the projectile line of flight at a position 167.6 cm behind the last detection station. A high-speed framing camera is placed so as to observe the projectile from a side view and to be perpendicular to the projectile line of flight. The camera is in line with the target's edge and xenon flash tube. The light from the xenon flash tube is directed by a Fresnel lens into the camera. During a firing the camera is operated at approximately 1,000,000 frames per second with the shutter open in a darkened room. With the arrival of the projectile at the target position, the xenon tube flashes allowing the high-speed camera to record the movement of the projectile and spray. About 20 useful frames are obtained for each firing. From the high-speed framing camera data the velocity of the projectile and target material spray, and the attitude of the projectile from a side view, are determined. Also, the shape of the spray cloud and the general particle size on the leading edge of the spray cloud are determined.

The chambers through which the projectile travels are evacuated to a pressure of 130 to 270 newtons/meter^2 to eliminate air drag on the projectile and to eliminate air interference with the experiment.

VIII. DISCUSSION AND PRESENTATION OF RESULTS

Analytical Development

The one-dimensional shock-wave theory in solids may be used to study the interaction of a projectile and thin target in collision. The theory is used here to construct a model which predicts the ratio of the maximum target material spray velocity and projectile impact velocity. An interaction model is developed to determine the variation of the maximum target material spray velocity with impact shock-wave pressure. The pressure from the impact shock wave in the thin target is then related to the necessary impact velocity of a projectile to produce this shock pressure.

A thin plate being penetrated by a high velocity disk is illustrated in figures 4(a) and 4(b). In figure 4(a) the projectile is penetrating into the thin target creating a shock wave in the target material traveling at velocity U_s. The shock wave in turn is accelerating the compressed target material to a velocity U_c. In figure 4(b) at a later time the shock wave is reflected from the free rear surface of the plate as an isentropic expansion wave. This isentropic expansion wave travels with the local speed of sound U_e into the compressed target material and produces relative to the compressed material velocity a velocity component U_r in the expanded material. In the laboratory coordinate system used in the figure the expansion wave travels at a velocity $U_e - U_c$ and the expanded target material has a velocity equal to the sum of U_c and U_r. The sum of U_c and U_r is the rear surface velocity U_f of the plate.

Thus,

$$U_f = U_c + U_r \tag{1}$$

For a shock pressure, the velocity component U_c is calculated by using the following two equations. The first of these equations is the experimentally obtained linear relation for commercial aluminum (ref. 4).

$$U_s = C' + C''U_c \tag{2}$$

U_s is the shock-wave velocity and C' and C'' are empirical constants for commercial aluminum. The second equation is the result of combining the mass and momentum equations for the Rankine-Hugoniot jump condition across a shock,

$$P_c - P_o = \rho_o U_s U_c \tag{3}$$

Here, the newly introduced quantities are P_c, the pressure in the compressed material after passage of the shock wave; P_o, the atmospheric pressure which in comparison to P_c is approximately zero; and ρ_o, the original density of the material at P_o. By using equation (2) to eliminate U_s in equation (3), and by picking a specific shock pressure P_c, the corresponding U_c may be calculated from the equation

$$U_c = \frac{-\left[\frac{C'}{C''}\right] + \sqrt{\left[\frac{C'}{C''}\right]^2 + \frac{4 P_c}{\rho_o C''}}}{2} \tag{4}$$

The velocity component U_r due to the isentropic expansion of the compressed material at the target's rear surface is the subject of an

extensive investigation for aluminum (refs. 8 and 9). It is shown (ref. 9) that the ratio U_r/U_c for a shock pressure between 100 and 500 kilobars (the region of interest in this investigation) in aluminum varies from 1.003 to 1.03. Therefore, the ratio U_r/U_c is taken as 1 in calculating U_r.

Then

$$U_r = U_c \tag{5}$$

Substituting for U_r in equation (1),

$$U_f = 2U_c \tag{6}$$

Thus, twice the compressed material velocity is taken to be the free rear surface velocity of the thin target for a shock pressure P_c.

The necessary impact velocity, U_p, to produce a certain shock pressure and associated free surface velocity in the target material for a tungsten projectile and aluminum target material combination, is now developed. Use is made of the boundary conditions at the projectile target interface. Across the interface the compressed projectile and target material have the same velocity and pressure. The similar velocity follows from the fact that there is no separation or intermixing of the compressed projectile and target material at the boundary. The equality of pressure follows from Newton's third law. Figure 5 shows graphically how use is made of these statements to determine the projectile velocity. The U_c versus P_c curves for the aluminum target material and tungsten projectile material are plotted. The curve sloping up from the left is for the target material and the

curve sloping up from the right is for the projectile material. The intersection of the two curves expresses during impact the equality of U_c and P_c of the compressed target and projectile material. The impact velocity of the projectile necessary to produce a specific U_c and P_c is obtained from the intersection of the P_c versus U_c curve of the projectile with the U_c coordinate.

Now, the impact velocity, U_p, is shown at the top of figure 5 to be composed of the sum of the compressed target material velocity, $\left(U_c\right)_t$, measured relative to the uncompressed target material velocity and the compressed projectile material velocity, $\left(U_c\right)_p$, measured relative to the uncompressed projectile material velocity. It should be noted at the top of figure 5 that $\left(U_c\right)_t = U_c$ and that $\left(U_c\right)_p \neq U_c$, where U_c is the compressed material velocity of both projectile and target measured relative to the laboratory coordinates.

Use is then made of equations

$$\left(U_c\right)_p = \frac{-\left[\frac{C_p'}{C_p''}\right] + \sqrt{\left[\frac{C_p'}{C_p''}\right]^2 + \frac{4\,P_c}{(\rho_o)_p C_p''}}}{2} \tag{7}$$

$$\left(U_c\right)_t = \frac{-\left[\frac{C_t'}{C_t''}\right] + \sqrt{\left[\frac{C_t'}{C_t''}\right]^2 + \frac{4\,P_c}{(\rho_o)_t C_t''}}}{2} \tag{8}$$

to calculate $\left(U_c\right)_p$ and $\left(U_c\right)_t$ for a specific P_c. The values of C_p' and C_p'' are taken from reference 7 for the projectile material. The sum of $\left(U_c\right)_p$ and $\left(U_c\right)_t$ is then constructed to determine the projectile impact velocity, U_p, corresponding to a shock-wave pressure, P_c.

Thus, by picking a certain P_c, the associated U_f may be determined and the necessary U_p may be determined.

Design of Experiment

In order to have the one-dimensional analysis hold during the impact process, the dimensions of the projectile and target must be carefully selected. The dimensions of the projectile are governed by the diameter of the gun barrel which is 0.56 cm in diameter and the ability of the gun to accelerate the thickest projectile possible without critically inhibiting its velocity performance.

The target thickness depends directly on the physical dimensions of the projectile. The target thickness is governed by the position at which the impact shock wave, traveling in the target material, is effected by rarefaction waves emanating from the rear and side of the projectile. These rarefaction waves are produced when the shock wave, propagating into the projectile, reaches the rear and side of the projectile and is reflected as rarefaction waves.

On the assumption that the impact between the face of the disk projectile and target is flat, calculations using Fowles' solution (ref. 5) show that rarefaction waves from the rear of the 0.038- and 0.076-cm-thick projectiles never affect the shock wave in the 0.0025- and 0.041-cm-thick aluminum targets. For the rarefaction waves emanating from the side of the projectile, the calculations using Bull's solution (ref. 1) show that the amount of the shock front affected for the case of 0.0025-cm-thick targets is less than 2 percent of the

projectile radius and for the 0.041-cm-thick targets is less than 20 percent of the projectile radius for all cases covered in the experiment.

The selection of the aluminum target and tungsten projectile material combination is based on several considerations. First, the Hugoniot curves are in existence for aluminum (ref. 4) and tungsten (ref. 7). Second, the one-dimensional shock-wave theory predicts that the maximum aluminum spray velocity is greater than the tungsten disk impact velocity. This makes photographing the target spray very convenient, and allows differentiation of target spray and the projectile spray in the photographic data.

Comparison of Analytical and Experimental Results

The analytical ratio of U_f/U_p versus U_p is plotted on figures 6 and 7 as a solid line. The experimental ratio of maximum aluminum spray velocity and tungsten projectile impact velocity is tabulated in table I for the corresponding experimental impact velocity. The experimental points are plotted as circles on figure 6 for the 0.0025-cm-thick targets and figure 7 for the 0.041-cm-thick targets. The plotted experimental points agree with the predicted values for the experimental impact velocity range tested.

Representative photographs of the experimental data with the 0.0025-cm-thick targets are presented in figures 8 through 12. These figures are placed in order of increasing projectile impact velocity. The impact velocity range for these shots covers from 0.113 to 0.295 cm/μsec.

Figure 8 shows the 0.076-cm-thick tungsten disk impacting the target at 0.113 cm/μsec. At +2.26 μsec after impact, a very fine mist is seen. By +9.04 μsec after impact this mist is dispersed, being invisible to the camera. Following this mist is a discrete particle of aluminum material. The velocity of this aluminum particle is the quantity used for the maximum spray velocity. Also, the tungsten disk can be seen intact at the back of the spray cloud. The ratio of maximum target material spray velocity and projectile impact velocity is 1.52.

Figure 9 is a photograph of the 0.076-cm-thick tungsten disk impacting at 0.179 cm/μsec. The disk is slightly but distinctly separated from the nylon sabot. In these photographs there is an air shock wave preceding the projectile and the spray. The air shock wave has very little effect on the maximum aluminum spray velocity, as verified by the fact that the ratio of the maximum aluminum spray velocity and projectile impact velocity is 1.59, which is very similar to that of other tests where no air shock waves could be seen. The leading portion of the spray cloud appears to be composed of a number of particles.

Figure 10 shows the 0.076-cm-thick tungsten disk impacting at 0.219 cm/μsec. Here, the cloud of target spray material is more finely fragmented than in the previous two figures. Preceding the dense cloud of particles is a fine mist of particles and several tiny jets. The maximum velocity of the spray cloud is taken as the boundary of the very dense region. The ratio of the maximum target material spray velocity and projectile impact velocity is 1.74.

Figure 11 shows the only experimental data which radically departs from the other experimental points and the predicted results. Two long dagger-shaped sprays have a tip velocity of 2.42 times the impact velocity. Their presence could be explained by either surface irregularities on the target and projectile or a possible contaminant. However, because of the very large development of the twin daggers with no other prominent spray features being present, the result is included in the plot for comparison with the predicted value.

Figure 12 shows a 0.038-cm-thick disk impacting at the highest velocity in the tests, 0.295 cm/μsec. The 0.038-cm-thick projectile acts in the same manner as the 0.076-cm-thick projectile in insuring that the one-dimensional condition is maintained a sufficient length of time in the target for the maximum target material spray velocity to be produced. The aluminum target material is very finely fragmented and followed by the slightly fragmented tungsten disk. Here, the ratio of maximum aluminum spray velocity and projectile impact velocity is 1.69.

The 0.0025-cm-thick aluminum targets provide a test of the sensitivity of the framing camera and xenon flash tube backlighting system. The sensitivity of this system is demonstrated by figures 8 through 12 where the aluminum sprays produced from extremely thin 0.0025-cm-thick targets are clearly visible to the camera over the impact velocity range tested. In fact, the test setup appears to be sufficiently sensitive to record the spray from targets thinner than 0.0025 cm. This experimental result indicates that when measurements are made for the

position of the leading edge of the spray cloud for the 0.041-cm-thick targets, the leading position of the first 0.0025 cm of target material can be measured.

Figures 13 through 18 are arranged with increasing projectile velocity for impacts into the 0.041-cm-thick targets. The impact velocity range covers from 0.089 to 0.291 cm/μsec. Figure 13 shows the lowest impact velocity, 0.089 cm/μsec, achieved with the 0.076-cm-thick projectiles in the experiments. At the front of the spray cloud is a large particle of the aluminum target. This is shown quite clearly at +8.24 μsec and +17.53 μsec after impact. This particle may be seen to exhibit rotation as it traverses the field of view. Here, the ratio of maximum target material spray velocity and projectile impact velocity is 1.48.

Figure 14 shows a slightly higher impact velocity of 0.143 cm/μsec using the 0.076-cm-thick projectile. A discrete particle of aluminum target material is leading the spray +12.84 μsec after impact. It can be noted that the 0.0025-cm-thick targets at this impact velocity did not fragment the tungsten projectile. However, in penetrating the thicker 0.041-cm-thick targets, the projectile is fractured and appears as a trapezoid with base forward in about the center of the spray cloud at +12.84 μsec after impact. The ratio of maximum target material spray velocity and projectile impact velocity is 1.58.

Figure 15 shows an impact velocity of 0.209 cm/μsec with the 0.076-cm-thick projectile. Here, the leading spray is composed of many small fragments. The fractured tungsten disk may again be seen in the

center of the spray cloud. The ratio of maximum target material spray velocity and projectile impact velocity is 1.59.

Figure 16 is included in the series to illustrate a very rapidly moving jet at the top of the leading portion of the spray cloud. The jet may be seen at +2.30 μsec and +4.60 μsec after impact of the 0.076-cm-thick projectile. However, at +9.20 μsec after impact, the jet is too dispersed to be seen by the camera. The flattened leading portion of the spray cloud is taken to be the maximum target material spray velocity. Further back in the spray cloud is the shattered projectile. The ratio of the maximum target material spray velocity and projectile impact velocity is 1.62.

Figure 17 shows an impact of the 0.076-cm-thick projectile at 0.250 cm/μsec. Again, the leading portion of the spray and the projectile are fragmented. The ratio of the maximum target material spray velocity and projectile impact velocity is 1.59.

Figure 18 shows the highest impact velocity, 0.291 cm/μsec, into the 0.041-cm-thick targets. This velocity is reached with the 0.038-cm-thick projectile. Again, this change in projectile thickness does not affect the maximum target material spray velocity which is of primary interest here. The frames at +7.91 μsec and +9.04 μsec after impact show twin jets preceding the main body of the spray. Their velocity is not taken as the maximum target material spray velocity. The leading edge of the elliptically shaped cloud is taken as the maximum target material spray velocity. For this shot the ratio of the maximum target material spray velocity and projectile velocity is 1.62.

It may be noted now that the impacts into the very thin 0.0025-cm-thick targets produce spray clouds which show very little lateral expansion of the target material spray, while the impacts into the thicker 0.041-cm-thick targets produce the familiar elliptically shaped cloud profiles. The lateral dispersion of the target material after the penetration of the 0.041-cm-thick targets illustrates the effect of the lateral rarefaction wave in the target. Another point to be noted is the requirement for a flat impact between the target and projectile faces to generate experimentally a one-dimensional flow in the target. The conditions in figure 19 are almost identical with those of figure 18 except for the projectile attitude which is very skewed in figure 19. The resulting ratio of maximum aluminum spray velocity and projectile impact velocity is equal to 1 for the skewed disk impact, as compared to 1.62 for the unskewed disk impact.

IX. CONCLUSIONS

It is possible to accelerate very dense disk-shaped projectiles unskewed and intact to high velocity. This allows the interaction of a thin bumper target and impacting projectile to be correlated with the one-dimensional shock-wave theory. The predicted result from the one-dimensional shock-wave theory, that the maximum target material spray velocity would be much greater than the impacting projectile velocity for the cases tested, is attained. Agreement between the experiments and theory is shown for the ratio of maximum target material spray velocity and projectile impact velocity. The agreement between the predicted and experimental results justifies the interaction model used.

Finally, the photographic records show greater fragmentation of the target material as the projectile impact velocity is increased.

X. SUMMARY

The maximum target material spray velocity emanating from the rear of a penetrated thin target is studied utilizing the one-dimensional shock-wave theory. A set of experiments is designed to evaluate the analytical results. The targets are 0.0025-cm-thick 1100 aluminum foil and 0.041-cm-thick 1100 H14 aluminum plate. The projectiles are made of tungsten and disk shaped. Their diameter is 0.56 cm and their thickness is either 0.076 or 0.038 cm. The projectile and target dimensions assure that the one-dimensional assumptions in the theory are valid. The impact velocity range is from 0.089 to 0.295 cm/μsec.

A method is developed to launch unskewed and intact very dense disk-shaped projectiles to high velocity. By using very dense tungsten projectiles the maximum aluminum target material spray velocity is as predicted by the theory well in excess of the projectile impact velocity. A ratio is defined as the maximum target material spray velocity to projectile impact velocity. The experimental ratio points are seen to agree with the predicted values for the impact velocity range covered.

Photographic data are presented and analyzed for the fragmentation of material on the leading edge of the target material spray cloud. As the impact velocity is increased the complete fragmentation of material on the leading edge is shown in the photographic data.

XI. ACKNOWLEDGMENTS

The author wishes to express his appreciation to the National Aeronautics and Space Administration which supported the research on which this thesis was written. In addition, the author wishes to express his appreciation to Dr. R. Thomas Davis and to the staff of the Engineering Mechanics Department of Virginia Polytechnical Institute for their guidance and criticism.

XII. REFERENCES

1. Bull, G. V.: On the Impact of Pellets With Thin Plates. Theoretical Considerations - Part 1. McGill University Technical Note 1-10-61.

2. Collins, Rufus D., Jr.; and Kinard, William H.: The Dependency of Penetration on the Momentum Per Unit Area of the Impacting Projectile and the Resistance of Material to Penetration. NASA TN-238, 1960.

3. Davidson, John R.; and Sandoff, Paul E.: Environmental Problems of Space Flight Structures. NASA TN D-1493, 1963.

4. Duvall, G. E.; and Fowles, G. R.: High Pressure Physics and Chemistry. R. S. Bradley, ed., Academic Press (London and New York), 1963, vol. II, pp. 209-291.

5. Fowles, G. R.: Attenuation of the Shock Wave Produced in a Solid by a Flying Plate. Journal of Applied Physics, vol. 31, no. 4, April 1960, pp. 655-661.

6. Humes, Donald H.: An Experimental Investigation of the Effectiveness of Single Aluminum Meteoroid Bumpers. NASA TN D-1784, May 1963.

7. McQueen, R. G.; and Marsh, S. P.: Equation of State for Nineteen Metallic Elements From Shock-Wave Measurements to Two Megabars. Journal of Applied Physics, vol. 31, no. 7, July 1960, pp. 1253-1269.

8. Walsh, J. M.; and Christian, R. H.: Equation of State of Metals From Shock Wave Measurements. Physical Review, vol. 97, no. 6, March 15, 1955, pp. 1544-1556.

9. Walsh, John M.; Rice, Melvin H.; McQueen, Robert G.; and Yarger, Frederick L.: Shock Wave Compression of Twenty-Seven Metals. Equations of State of Metals. Physical Review, vol. 108, no. 2, October 15, 1957, pp. 196-216.

10. Whipple, Fred L.: Meteoritic Phenomena and Meteorites. Physics and Medicine of the Upper Atmosphere. Clayton S. White and Otis O. Benson, Jr., eds., The Univ. of New Mexico Press (Albuquerque), 1952, pp. 137-170.

The vita has been removed from the scanned document

TABLE I.- TABULATED DATA

Target properties			Projectile properties				Projectile velocity	Maximum spray velocity / Projectile velocity
Shot number	Material	Thickness (cm)	Material	Shape	Diameter (cm)	Thickness (cm)	(cm/μsec)	
1	1100 aluminum	0.0025	Tungsten	Disk	0.56	0.076	0.113	1.52
2	1100 aluminum	.0025	Tungsten	Disk	.56	.076	.135	1.55
3	1100 aluminum	.0025	Tungsten	Disk	.56	.076	.179	1.59
4	1100 aluminum	.0025	Tungsten	Disk	.56	.076	.219	1.74
5	1100 aluminum	.0025	Tungsten	Disk	.56	.076	.243	2.42
6	1100 aluminum	.0025	Tungsten	Disk	.56	.038	.295	1.69
7	1100 H14 aluminum	.041	Tungsten	Disk	.56	.076	.089	1.48
8	1100 H14 aluminum	.041	Tungsten	Disk	.56	.076	.137	1.68
9	1100 H14 aluminum	.041	Tungsten	Disk	.56	.076	.143	1.58
10	1100 H14 aluminum	.041	Tungsten	Disk	.56	.076	.162	1.71
11	1100 H14 aluminum	.041	Tungsten	Disk	.56	.076	.209	1.59
12	1100 H14 aluminum	.041	Tungsten	Disk	.56	.076	.212	1.62
13	1100 H14 aluminum	.041	Tungsten	Disk	.56	.076	.250	1.59
14	1100 H14 aluminum	.041	Tungsten	Disk	.56	.076	.270	1.65
15	1100 H14 aluminum	.041	Tungsten	Disk	.56	.076	.273	1.76
16	1100 H14 aluminum	.041	Tungsten	Disk	.56	.038	.291	1.62
17	1100 H14 aluminum	.041	Tungsten	Disk	.56	.038	.294	1.00

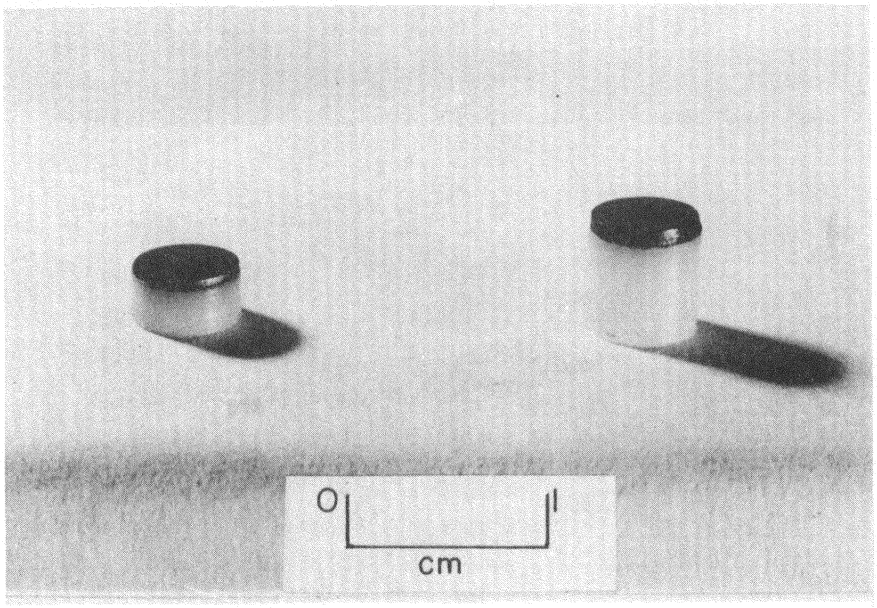

Left projectile

Tungsten disk

.56 cm in diameter

.038 cm in thickness mounted on nylon sabot

.56 cm in diameter

.28 cm in thickness

Right projectile

Tungsten disk

.56 cm in diameter

.076 cm in thickness mounted on nylon sabot

.56 cm in diameter

.56 cm in thickness

Figure 1.- Projectiles mounted for firing.

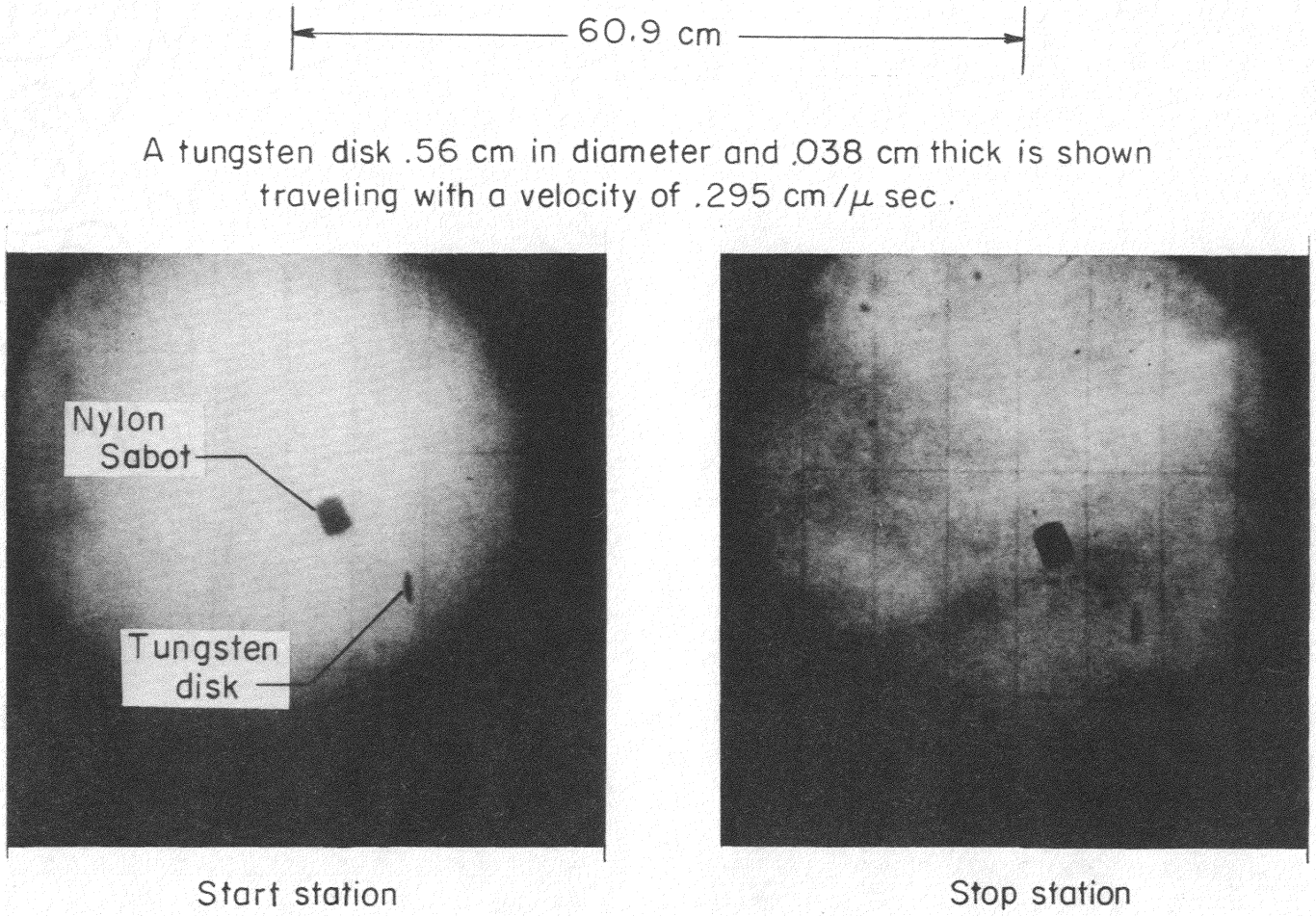

Figure 2.- Projectile photographs taken at the two detection stations.

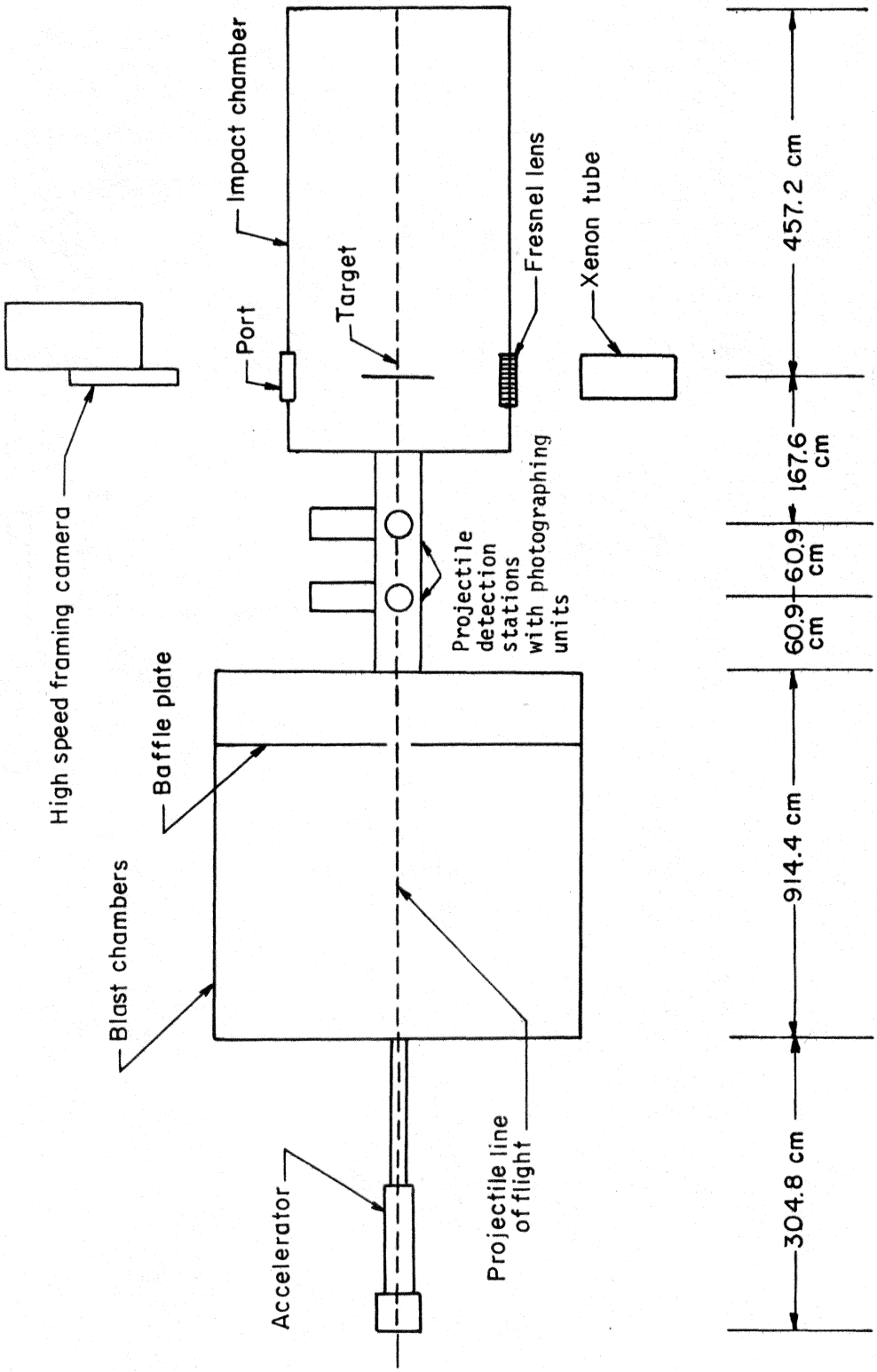

Figure 3.- Schematic drawing of experimental setup.

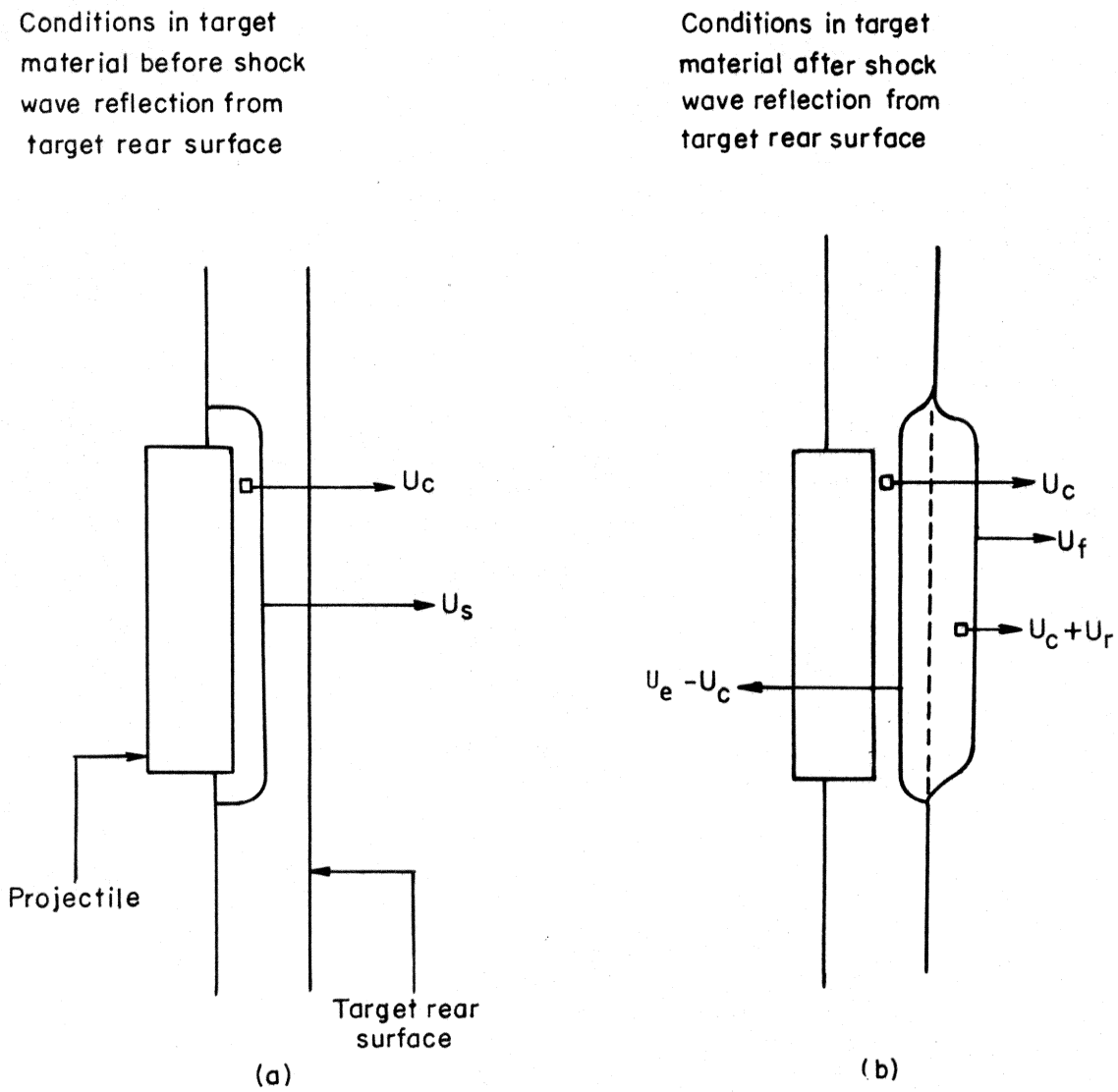

Figure 4.- Conditions produced in target with impact of projectile.

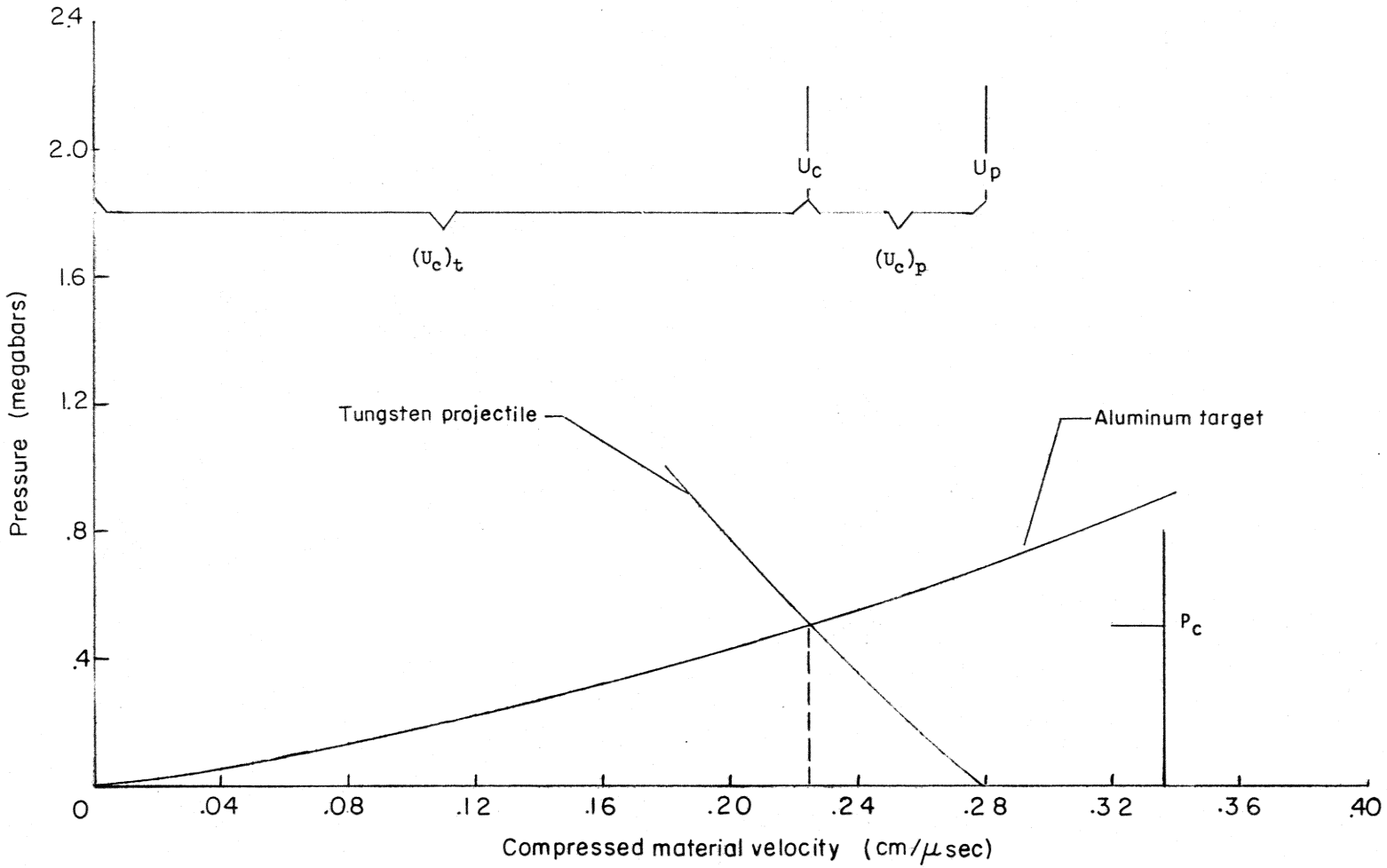

Figure 5.- Graphical solution to determine projectile impact velocity.

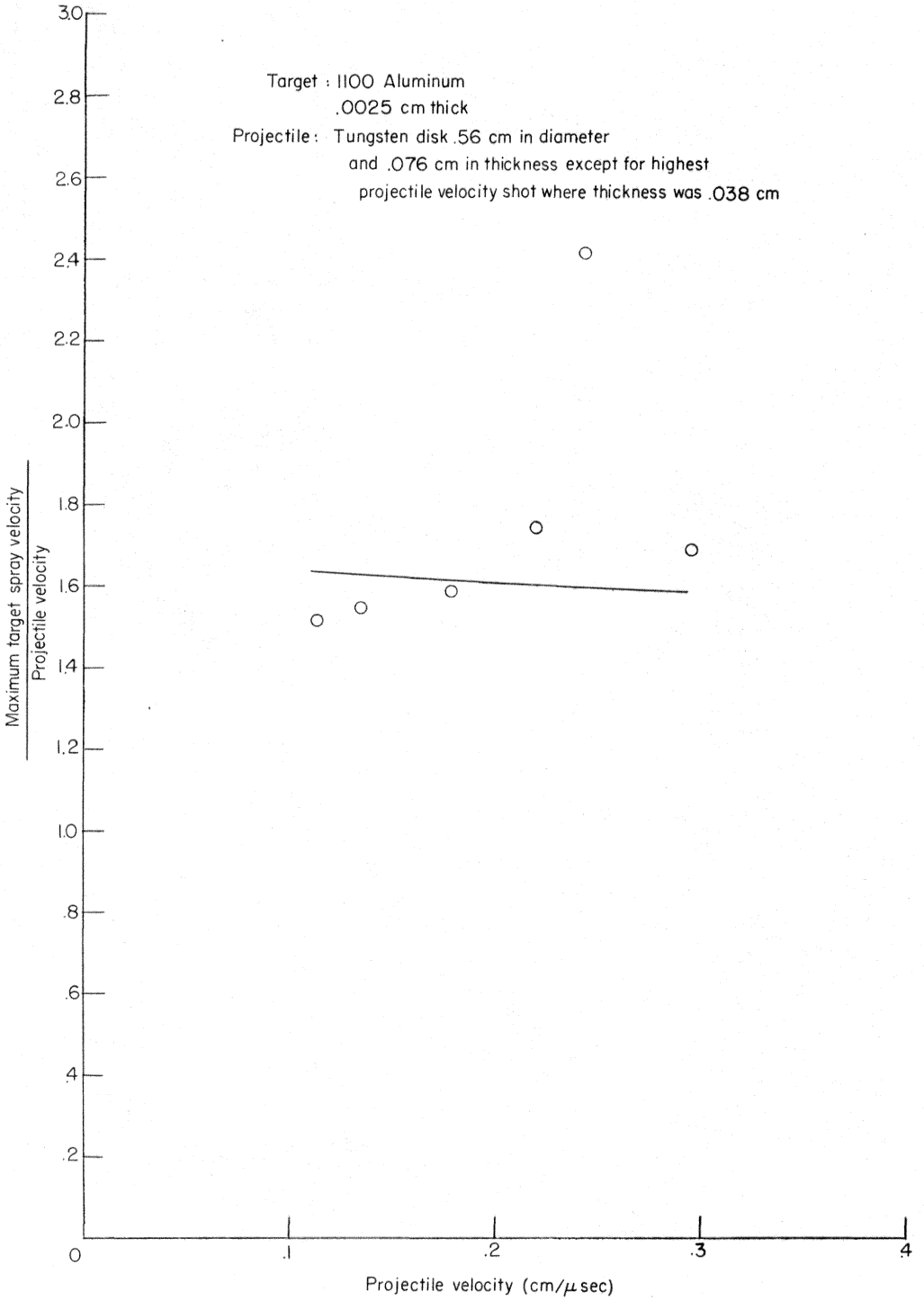

Figure 6.- Comparison of experimental and predicted ratio of maximum target-material spray velocity and projectile velocity.

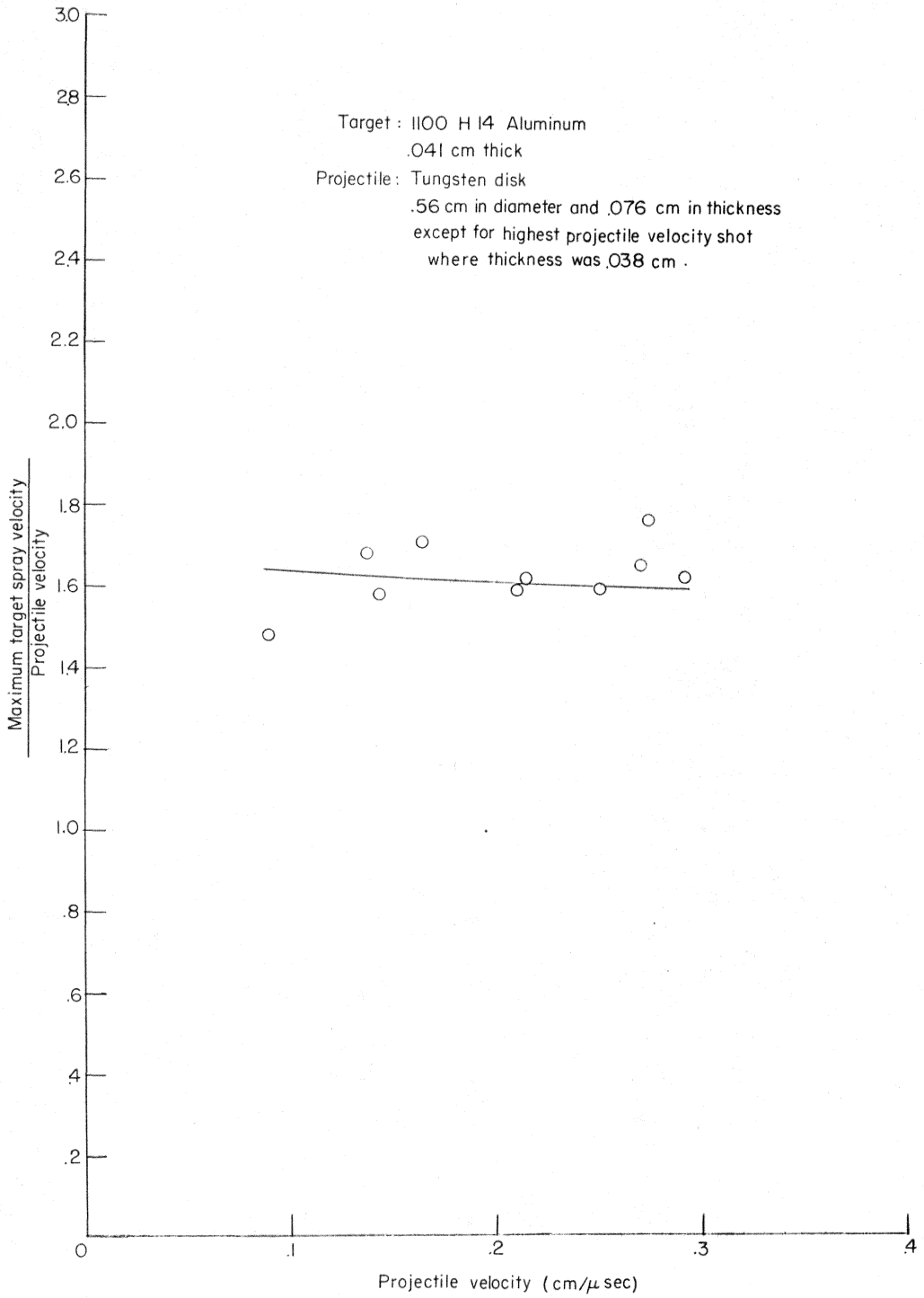

Figure 7.- Comparison of experimental and predicted ratio of maximum target-material spray velocity and projectile velocity.

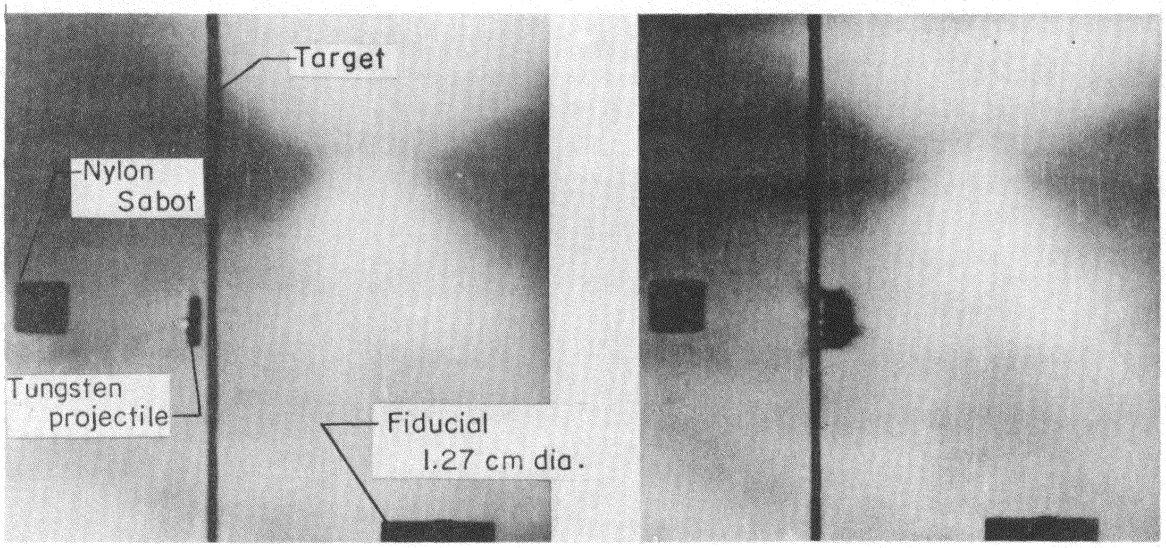

$-1.13\ \mu$ sec $+2.26\ \mu$ sec

The maximum ratio of target material spray velocity and projectile impact velocity is 1.52 .

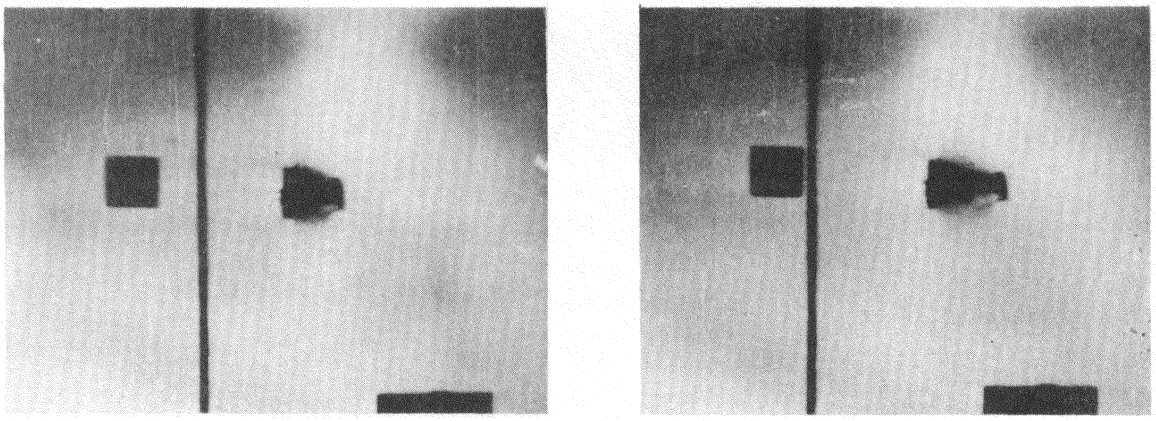

$+9.04\ \mu$ sec $+12.43\ \mu$ sec

Shot no. 1

Figure 8.- A tungsten disk 0.56 cm in diameter and 0.076-cm-thick impacting an aluminum 1100 target 0.0025-cm-thick at 0.113 cm/μsec.

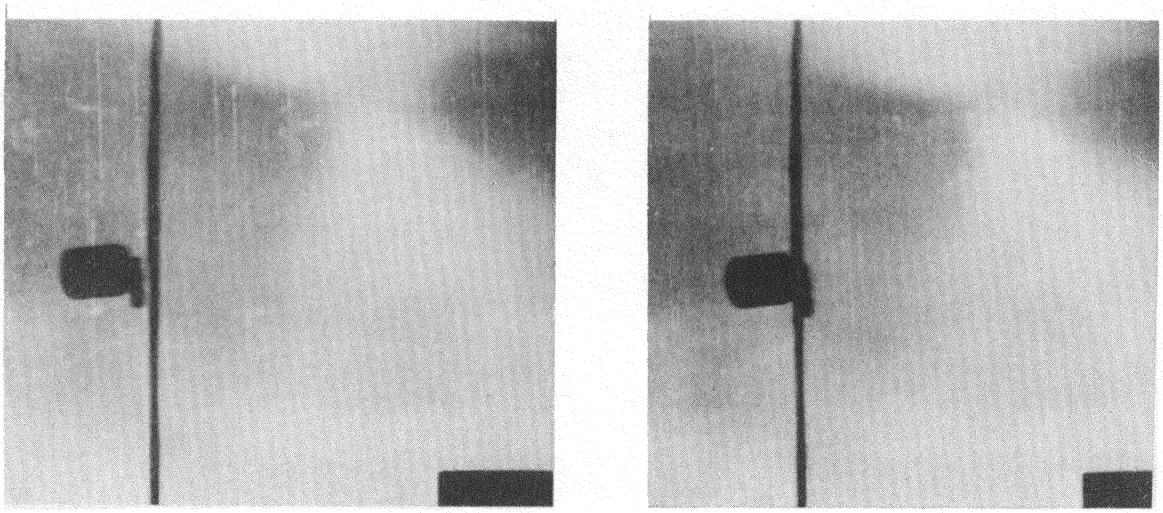

-1.33 μ sec

+0.00 μ sec

The maximum ratio of target material spray velocity and projectile impact velocity is 1.59. Note also shock wave proceding projectile and also spray.

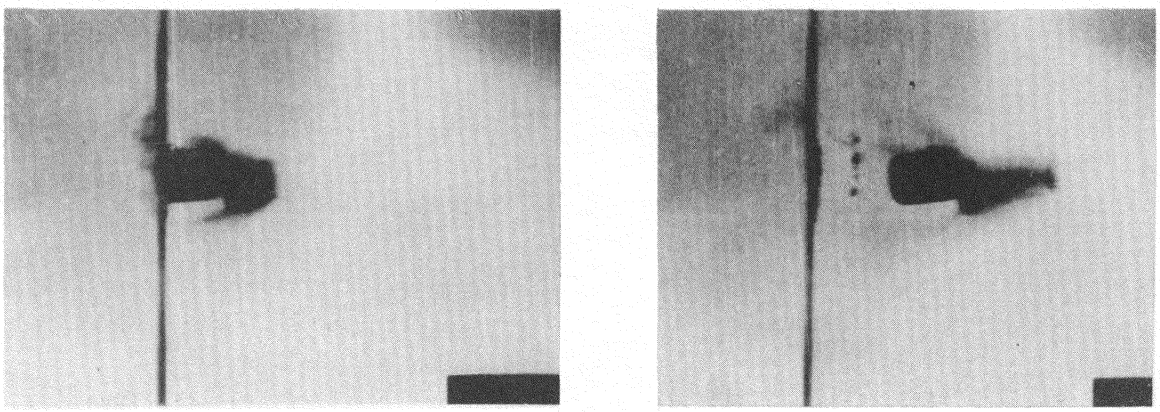

+ 3.99 μ sec

+ 9.31 μ sec

Shot no. 3

Figure 9.- A tungsten disk 0.56 cm in diameter and 0.076-cm-thick impacting an aluminum 1100 target 0.0025-cm-thick at 0.179 cm/μsec.

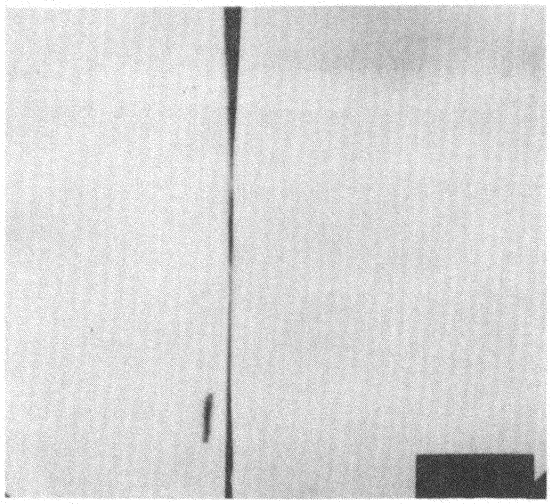

-0.00μ sec

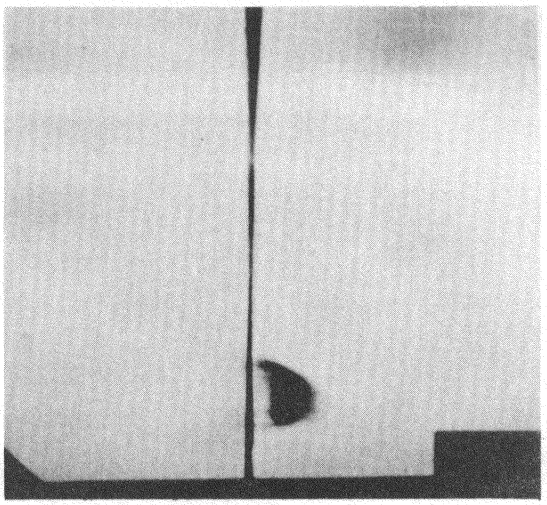

+ 2.38 μ sec

The maximum ratio of target material spray velocity and projectile impact velocity is 1.74 .

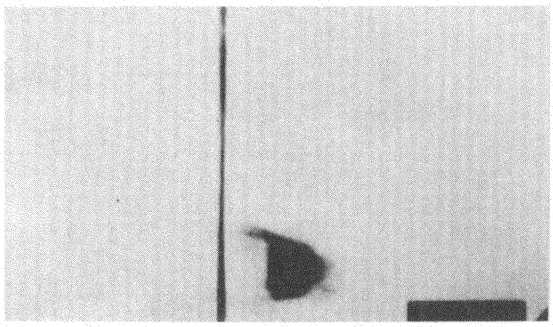

+ 3.57 μ sec

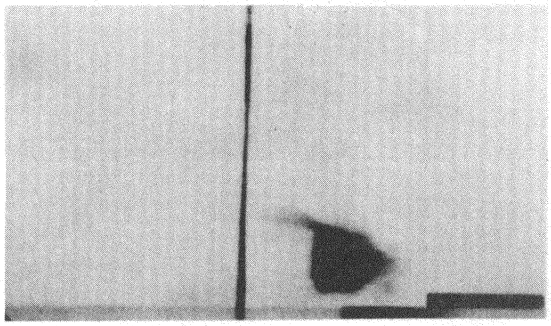

+ 4.76 μ sec

Shot no. 4

Figure 10.- A tungsten disk 0.56 cm in diameter and 0.076-cm-thick impacting an aluminum 1100 target 0.0025-cm-thick at 0.219 cm/μsec.

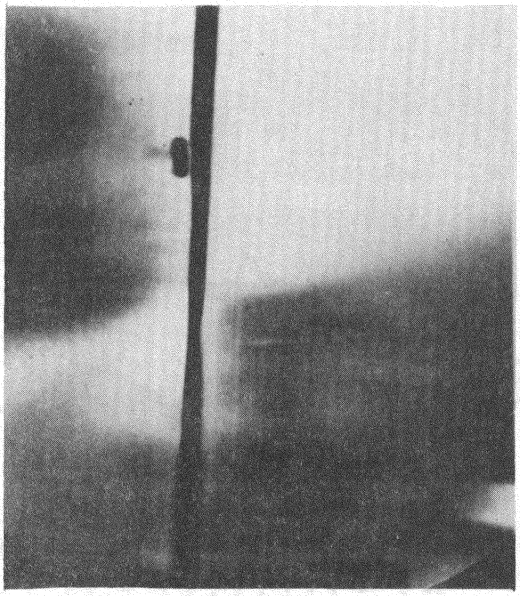

−0.00 μ sec

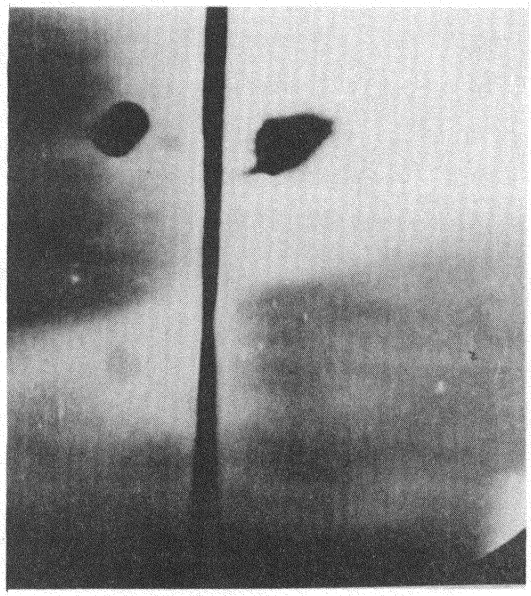

+ 4.04 μ sec

The maximum ratio of target material spray velocity and projectile impact velocity is 2.42.

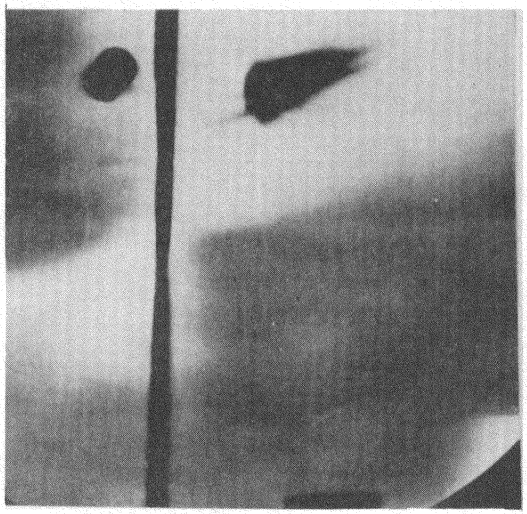

+ 6.06 μ sec

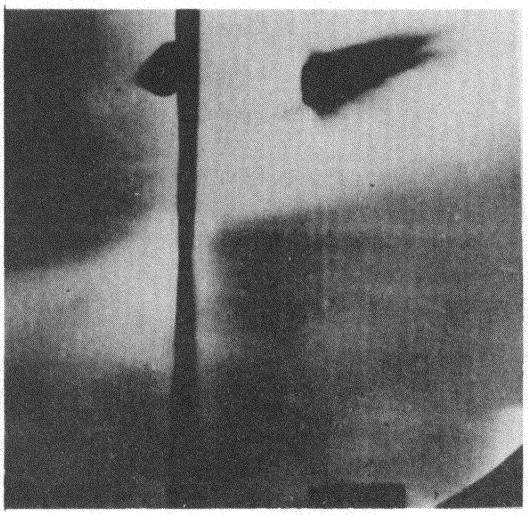

+ 8.08 μ sec

Shot no. 5

Figure 11.- A tungsten disk 0.56 cm in diameter and 0.076-cm-thick impacting an aluminum 1100 target 0.0025-cm-thick at 0.243 cm/μsec.

− 1.15 μ sec

+ 1.15 μ sec

The maximum ratio of target material spray velocity and projectile impact velocity is 1.69.

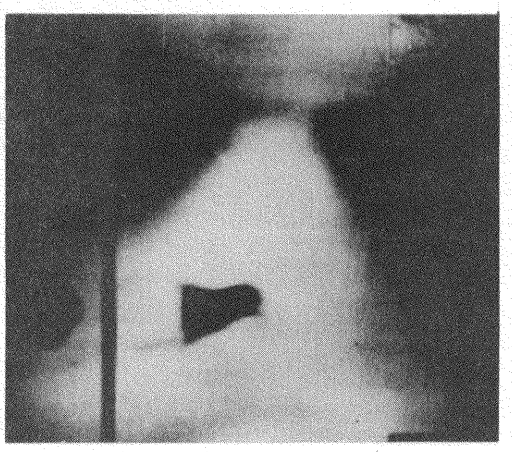

+ 3.45 μ sec

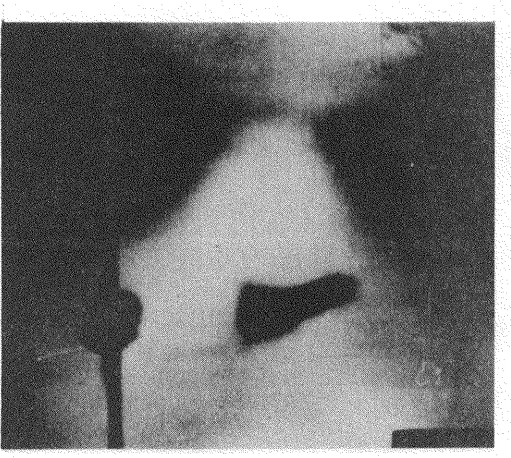

+ 5.75 μ sec

Shot no. 6

Figure 12.- A tungsten disk 0.56 cm in diameter and 0.038-cm-thick impacting an aluminum 1100 target 0.0025-cm-thick at 0.295 cm/μsec.

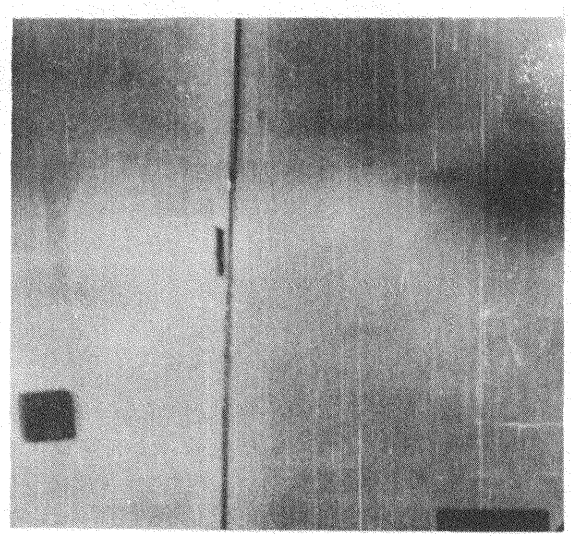

−1.03 μ sec

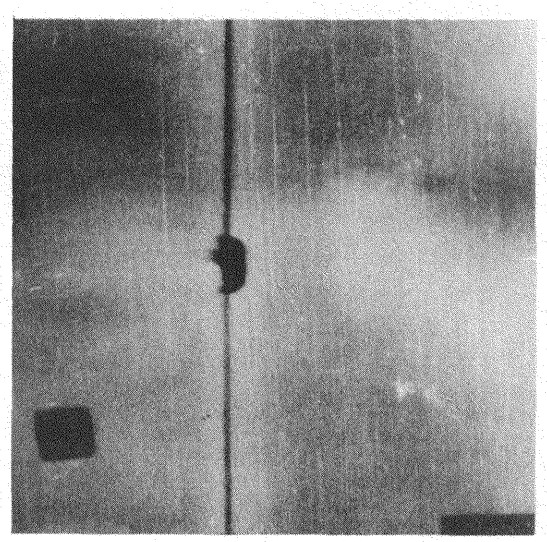

+1.03 μ sec

The maximum ratio of target material spray velocity and projectile impact velocity is 1.48.

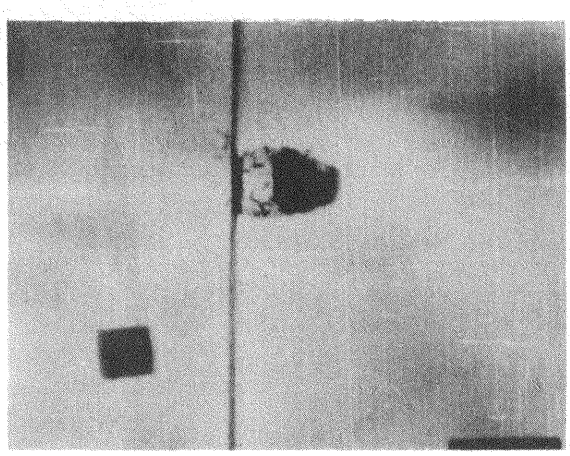

+8.24 μ sec

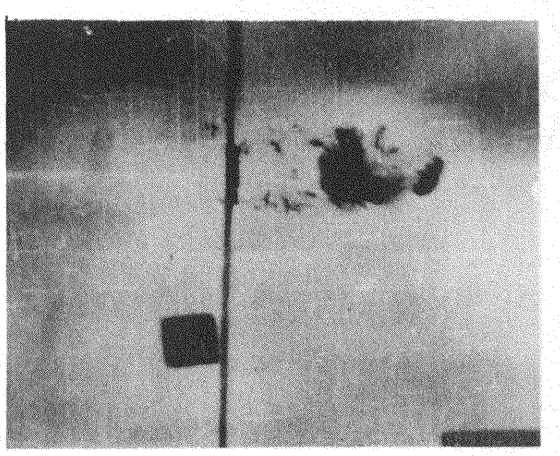

+17.53 μ sec

Shot no. 7

Figure 13.- A tungsten disk 0.56 cm in diameter and 0.076-cm-thick impacting an aluminum 1100 H14 target 0.041-cm-thick at 0.089 cm/μsec.

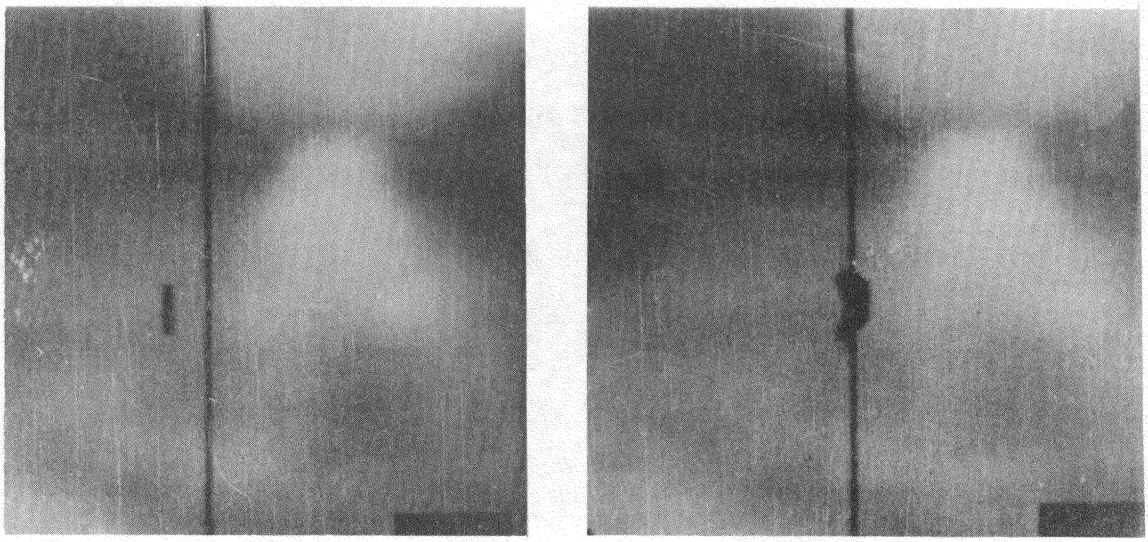

$-2.14\ \mu$ sec $+1.07\ \mu$ sec

The maximum ratio of target material spray velocity and projectile impact velocity is 1.58.

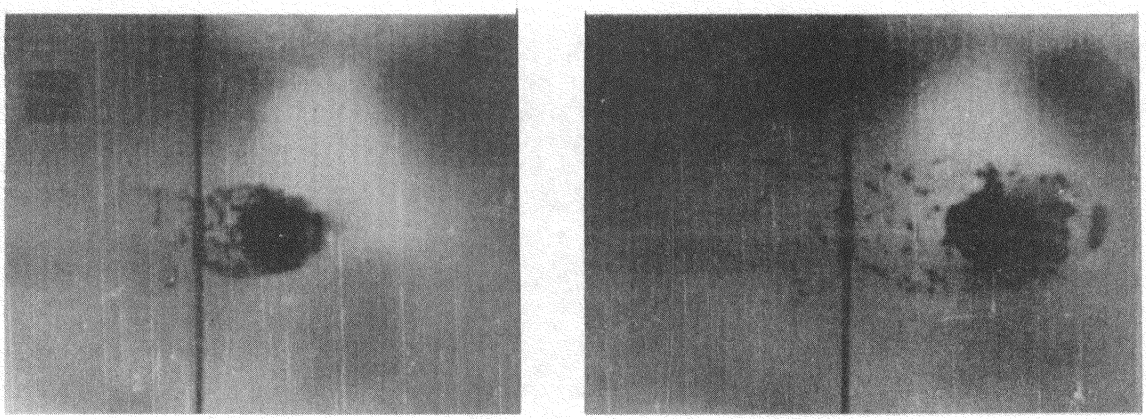

$+6.42\ \mu$ sec $+12.84\ \mu$ sec

Shot no. 9

Figure 14.- A tungsten disk 0.56 cm in diameter and 0.076-cm-thick impacting an aluminum 1100 H14 target 0.041-cm-thick at 0.143 cm/μsec.

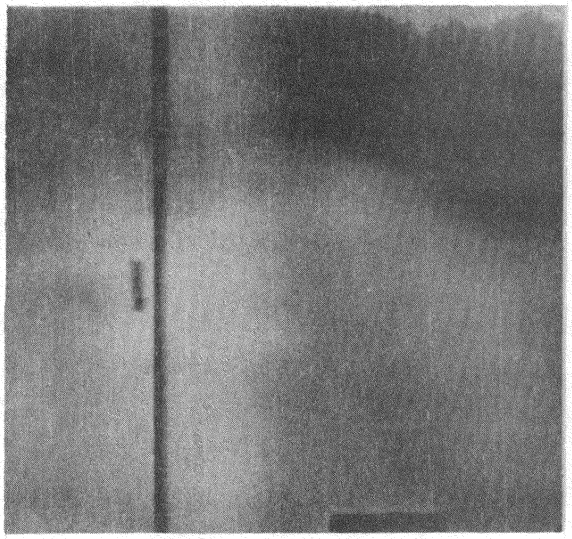

−1.10 μ sec

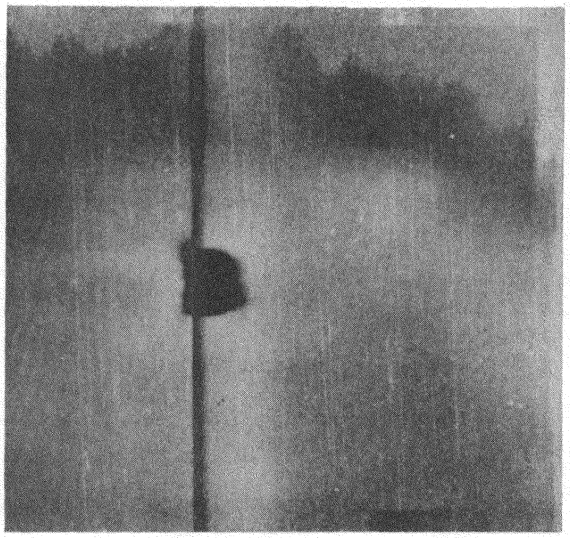

+1.10 μ sec

The maximum ratio of target material spray velocity and projectile impact velocity is 1.59.

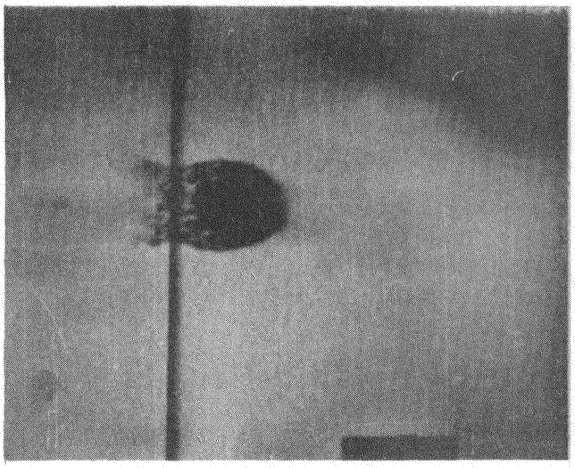

+ 3.30 μ sec

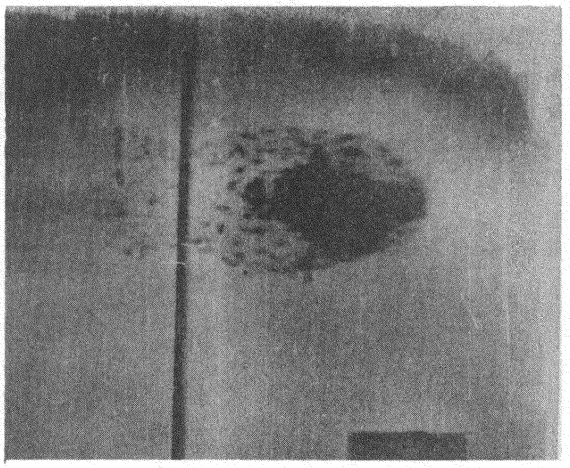

+ 7.70 μ sec

Shot no. 11

Figure 15.- A tungsten disk 0.56 cm in diameter and 0.076-cm-thick impacting an aluminum 1100 H14 target 0.041-cm-thick at 0.209 cm/μsec.

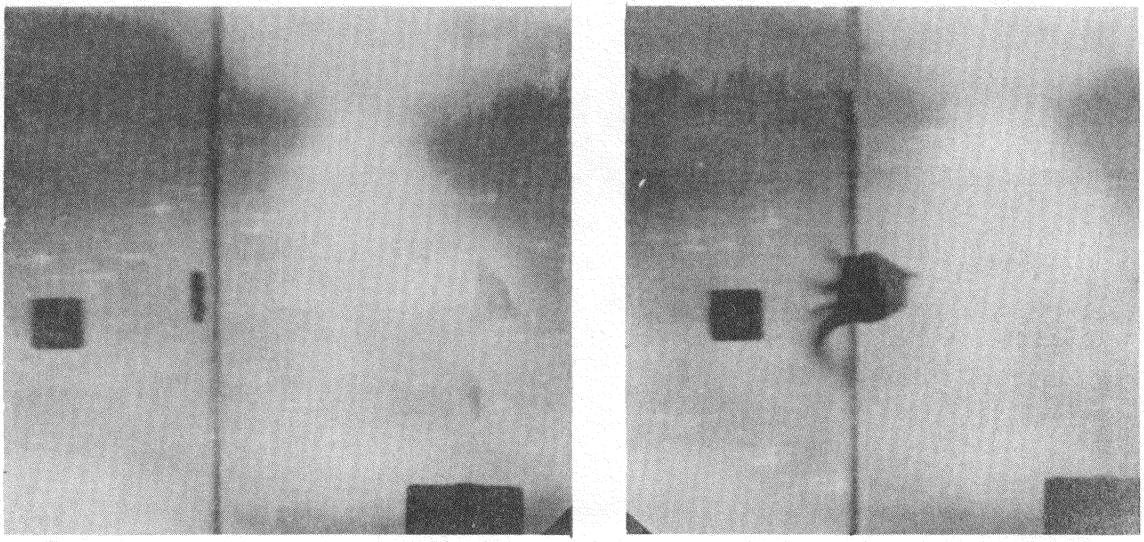

$-0.00\ \mu$ sec $+2.30\ \mu$ sec

The maximum ratio of target material spray velocity and projectile impact velocity is 1.62.

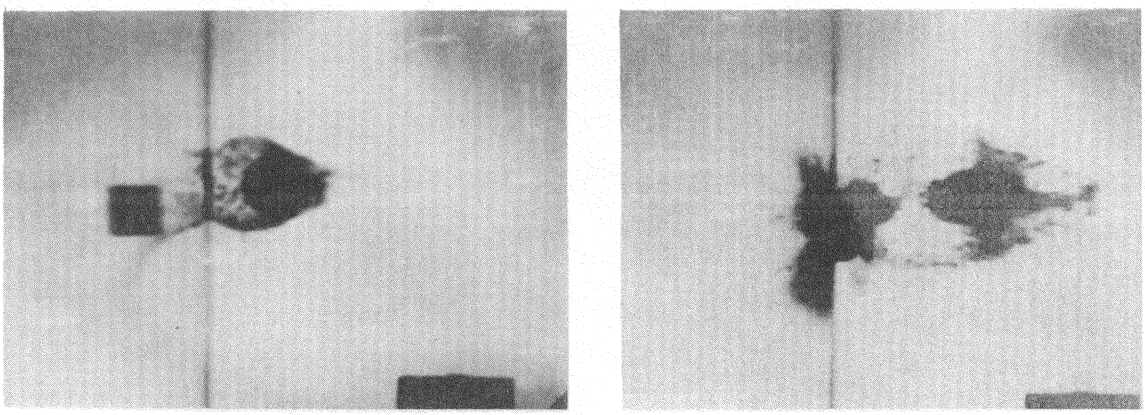

$+4.60\ \mu$ sec $+9.20\ \mu$ sec

Shot no. 12

Figure 16.- A tungsten disk 0.56 cm in diameter and 0.076-cm-thick impacting an aluminum 1100 H14 target 0.041-cm-thick at 0.212 cm/μsec.

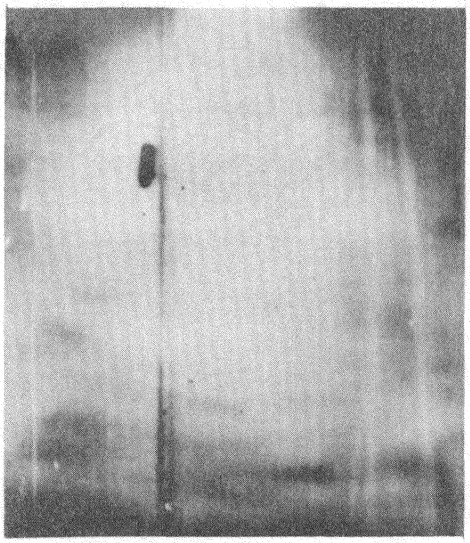

−0.00 μ sec

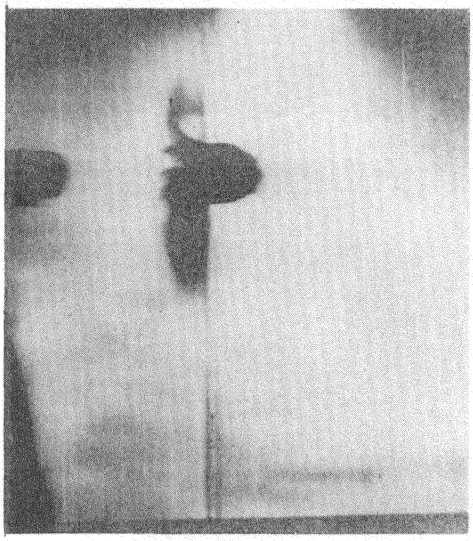

+ 2.00 μ sec

The maximum ratio of target material spray velocity and projectile impact velocity is 1.59 .

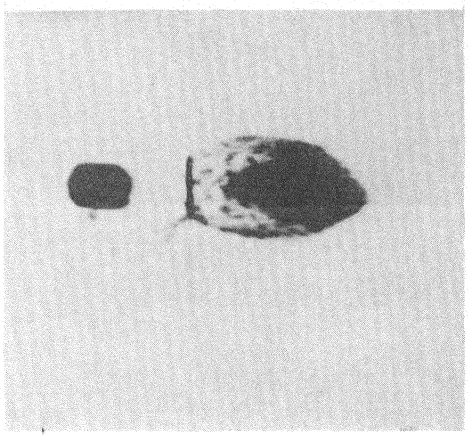

+ 6.00 μ sec

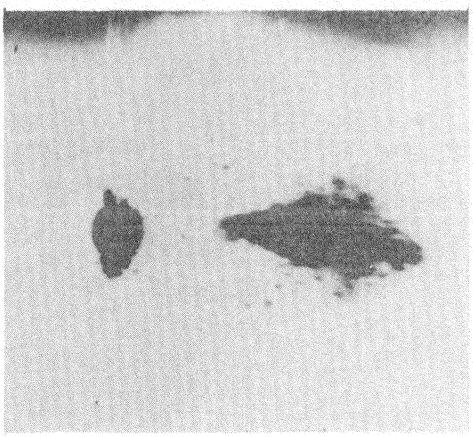

+ 10.00 μ sec

Shot no. 13

Figure 17.- A tungsten disk 0.56 cm in diameter and 0.076-cm-thick impacting an aluminum 1100 H14 target 0.041-cm-thick at 0.250 cm/μsec.

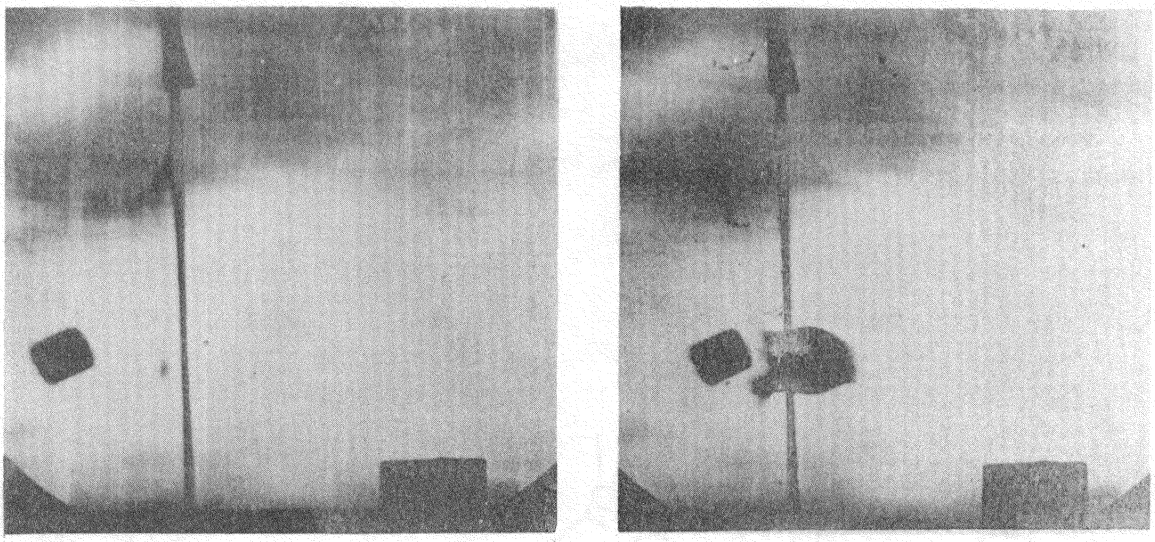

−0.00 μ sec

+ 2.26 μ sec

The maximum ratio of target material spray velocity and projectile impact velocity is 1.62 .

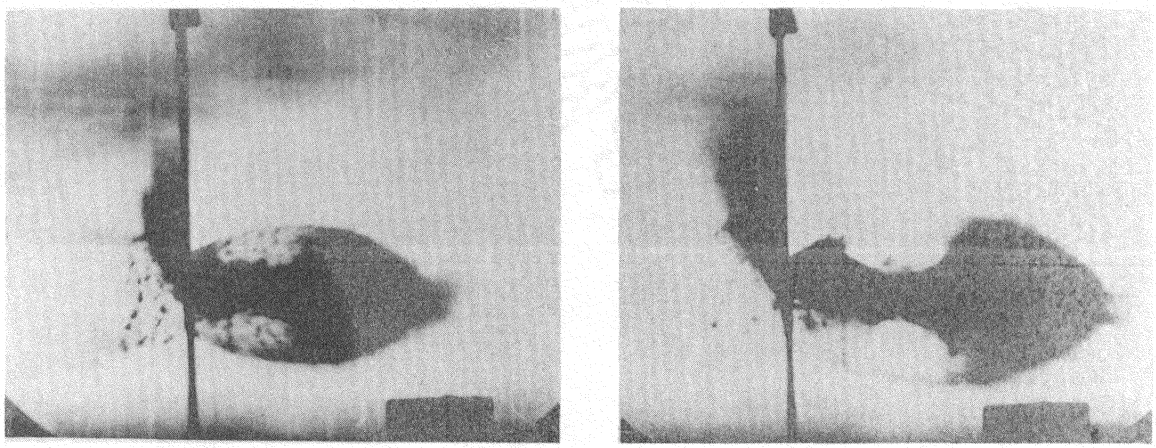

+7.91 μ sec

+ 9.04 μ sec

Shot no. 16

Figure 18.- A tungsten disk 0.56 cm in diameter and 0.038-cm-thick impacting an aluminum 1100 H14 target 0.041-cm-thick at 0.291 cm/μsec.

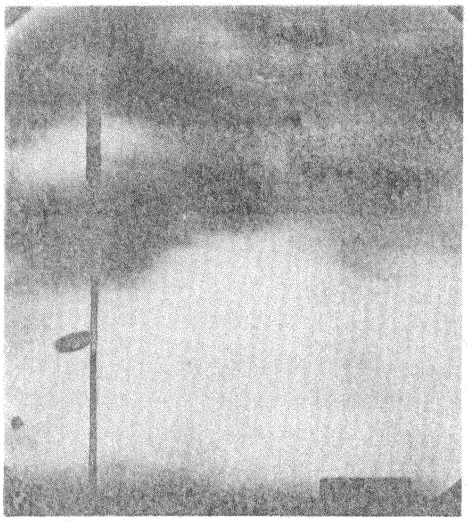

−0.00 μ sec

+6.82 μ sec

The maximum ratio of target material spray velocity and projectile impact velocity is 1 .

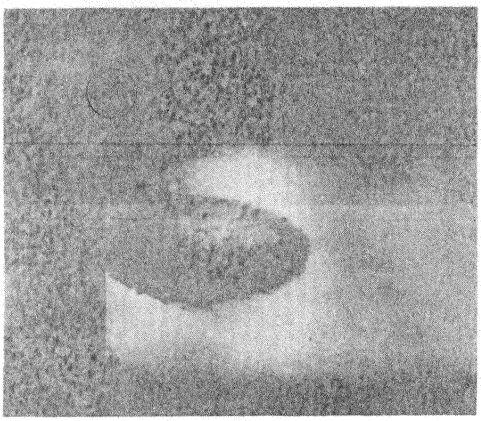

+10.26 μ sec

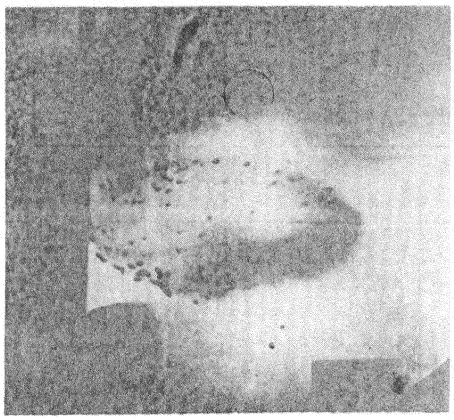

+13.68 μ sec

Shot no. 17

Figure 19.- A tungsten disk 0.56 cm in diameter and 0.038-cm-thick impacting an aluminum 1100 H14 target 0.041-cm-thick at 0.294 cm/μsec.

AN INVESTIGATION OF THE MAXIMUM TARGET MATERIAL SPRAY VELOCITY PRODUCED IN THE PENETRATION OF THIN PLATES BY HIGH VELOCITY DISKS

By

John D. Di Battista

ABSTRACT

The maximum target material spray velocity emanating from the rear of a penetrated thin target is studied utilizing the one-dimensional shock-wave theory. A set of experiments is designed to evaluate the analytical results. The targets are 0.0025-cm-thick 1100 aluminum foil and 0.041-cm-thick 1100 H14 aluminum plate. The projectiles are made of tungsten and disk shaped. Their diameter is 0.56 cm and their thickness is either 0.076 or 0.038 cm. The projectile and target dimensions assure that the one-dimensional assumptions in the theory are valid. The impact velocity range is from 0.089 to 0.295 cm/μsec.

A method is developed to launch unskewed and intact very dense disk-shaped projectiles to high velocity. By using very dense tungsten projectiles the maximum aluminum target material spray velocity is as predicted by the theory well in excess of the projectile impact velocity. A ratio is defined as the maximum target material spray velocity to projectile impact velocity. The experimental ratio points are seen to agree with the predicted values for the impact velocity range covered.

Photographic data are presented and analyzed for the fragmentation of material on the leading edge of the target material spray cloud. As the impact velocity is increased the complete fragmentation of material on the leading edge is shown in the photographic data.